DOI: 10.15480/882.9297

Eighth International Symposium on Marine Propulsors
smp'24, Berlin, Germany, March 2024

Analysis of the damping and added mass properties of the marine propeller

M. Maaz Abbasi[1], Adhil M. Asif[1], Lutz Kleinsorge[1], Gunnar Kistner[2]

[1]Mecklenburger Metallguss GmbH (MMG), Germany
[2] Faculty of Mechanical Engineering and Marine Technology, University of Rostock, Germany

ABSTRACT

Unsteady Reynolds-Averaged Navier-Stokes (RANS) simulations are performed on a full-scale marine propeller to obtain its torsional added mass and damping coefficients under various hydrodynamics conditions. These coefficients, also called propeller coefficients, originate from additional hydrodynamic forces and moments acting on the propeller in a non-uniform hull wakefield and are vital for torsional vibration calculations. A CFD model in the propeller open water test (OWT) condition is used in this paper for a full-scale propeller to obtain these coefficients. The effect of a nonuniform wakefield is numerically modeled by superimposing a torsional motion with a uniform flow, and the torsional vibration is numerically modeled by superimposing a harmonic torsional oscillation on the propeller's rotation motion in the propeller OWT condition. The propeller's resultant added mass and damping coefficients are computed and compared with available methods, such as Archer and Schwanecke. The influence of excitation frequency, advance ratio, and vibration magnitude on added mass and damping coefficients is studied. Moreover, the effect of the propeller's geometrical properties such as the pitch ratio, expanded area ratio, blade skew, and blade number on the propeller's coefficients are investigated.

Keywords

RANS, torsional added mass, torsional damping, CFD, propeller Open Water Test (OWT)

1 INTRODUCTION

A marine propeller operates in a non-uniform and rather complex wakefield behind the ship hull. The result of a complete propeller rotation in this wakefield are periodic forces being applied on the propeller blades whose period depends mainly on the blade passing frequency of the propeller. The addition of these results in an unsteady total thrust of the propeller which causes the propeller to vibrate. It happens locally on the propeller blade due to its elastic nature or on a more global scale as a part of the propulsion shafting system which includes the propeller shaft, intermediate shaft, and engine crankshaft. In this case, the propeller is considered as a rigid body moving in six degrees of freedom. The shafting vibration causes the propeller's surrounding fluid to accelerate and thus additional forces are generated due to this acceleration. These forces are found to be proportional to the magnitude of acceleration, velocity, and displacement of the vibration. The resulting constants are called added mass, damping, and stiffness of the propeller respectively (Carlton 2018).

From a structural point of view, the propeller vibration induces cyclic loading, and thus stresses on the shafting system along all 6 degrees of freedom. Among other stresses, torsional stress is of prime importance as the propulsion shafting carries a large torsional load from the engine towards the propeller where the propeller end is also loaded with hydrodynamic loads. Fluctuations in torsional loads, and thus torsional stresses, due to a non-uniform wakefield result in a reduced life of the shafting system because of the associated fatigue.

The propeller hydrodynamic coefficients play a vital role in correctly predicting the local response of the shafting system and its effect on the global hull vibration. In the past, experiments were performed to obtain torsional and longitudinal damping coefficients, see for example Archer (1951), Lewis et al. (1960), and Burrill & Robson (1962). The propeller characteristics were varied systematically in both torsional and longitudinal directions. The approach was then generalized for an arbitrary propeller by deriving a series of empirical expressions which take the propeller geometry and performance as an input.

A semi-empirical formulation by Schwanecke (1963) is often used in the literature to obtain the added mass and damping coefficients based on the propeller's geometrical characteristics by employing an unsteady propeller theory. The hydrodynamic reaction forces as a result of propeller oscillations were calculated using unsteady lifting surface theory used by Hyloarides & Van Gent (1979). It was shown that a linear relationship persisted between added mass and blade area ratio whereas pitch had a weaker dependency. The added mass and damping properties of marine propellers in all modes of vibrations were analyzed by Parsons et al. (1980) using two-dimensional thin foil theory to obtain the pressure distribution on the

propeller blade against a unit heave or pitch oscillation. It was found that added mass is less sensitive to the advance ratio than damping and an increase in excitation frequency increased the added mass while damping decreased. A low-order panel method was utilized by Gaschler & Abdel-Maksoud (2014) to study hydrodynamical mass and damping of propellers in heave motion in an open water condition for non-rotating, rotating, and cavitating propellers. Results showed that the damping coefficient in the vertical direction for the rotating case is much higher than the non-rotating case whereas the added mass remained the same. The influence of skew on added mass and damping properties of marine propellers was investigated by Mao & Young (2016). They found out that the skew affects the heave, sway, pitch, and yaw components of damping and added mass matrices. However, the influence on roll and surge is negligible. A numerical methodology was proposed by Li et al. (2018) to obtain the damping coefficient and added mass of the propeller by employing the 3D panel method. Results showed that the absolute value of added mass coefficients decreased as the ratio of oscillation frequency and blade frequency decreased. The absolute value of the damping coefficient increased with the advance ratio regardless of this frequency ratio.

The axial and torsional vibrations were performed using URANS by Van Esch et al. (2013). The authors computed the unsteady hydrodynamic torque for a single propeller in open water conditions. The result showed the influence of reduced frequency on the vibratory motion of the propeller. Moreover, URANS was also used to obtain the virtual mass and the damping coefficients of the model scale marine propeller for straight and oblique flow by Martio et al. (2015) and Martio et al. (2017). Results were in agreement with the semi-empirical model available in the literature.

The literature review suggests that in terms of propeller geometry, the blade area ratio, blade number, moment of inertia, and propeller skew influenced the propeller coefficients the most whereas the pitch showed weaker dependency, especially on the added mass coefficient. From the operational conditions' point of view the advanced ratio, propeller rotational speed, and excitation frequency were the main parameters that affect the propeller coefficients. This paper aims to investigate the behavior of added mass and damping coefficients due to operational and geometrical parameters.

2 METHODOLOGY

2.1 Theoratical background

In general, there are six vibration directions corresponding to six degrees of freedom for a rigid propeller acting as part of the shafting system as shown in Figure 1. The general equation of motion for the propeller with mass matrix 'M' vibrating in a uniform wakefield due to excitation force F_e with displacement '$x = [\delta_x, \delta_y \delta_z, \phi_x, \phi_y, \phi_z]^T$' as given by Carlton (2018) is:

$$M\ddot{x} = F_e + f_H \tag{1}$$

The hydrodynamic forces and moments (represented by the matrix f_H) as a result of vibration are found to be proportional to the magnitude of acceleration and velocity in the case of a fully submerged propeller. These forces oppose the motion of the propeller and are thus written in the following form:

$$f_H = -M_a\ddot{x} - C_p\dot{x} \tag{2}$$

Where M_a represents the added mass matrix. C_p represents the damping (propeller damping) matrix. Based on the coupling effect among various coordinate axes, the propeller vibration problem is mainly studied in two classes. They include axial-torsional motion and lateral vibration motion. For axial-torsional motion, only four unknowns are required for added mass $(m^*_{11}, m^*_{44}, m^*_{14}, m^*_{41})$ and damping matrix $(c^*_{11}, c^*_{44}, c^*_{14}, c^*_{41})$.

$$\begin{bmatrix} m^*_{11} & m^*_{14} \\ m^*_{41} & m^*_{44} \end{bmatrix} \cdot \begin{bmatrix} \ddot{x} \\ \ddot{\theta} \end{bmatrix} - \begin{bmatrix} c^*_{11} & c^*_{14} \\ c^*_{41} & c^*_{44} \end{bmatrix} \cdot \begin{bmatrix} \dot{x} \\ \dot{\theta} \end{bmatrix} = \begin{bmatrix} f_{H_x}(t) \\ q_{H_x}(t) \end{bmatrix} \tag{3}$$

The harmonic oscillations at a given time t are prescribed in the torsional direction to obtain the respective added mass and damping coefficients.

$$\theta(t) = \theta_0 sin(\omega \cdot t) \tag{4}$$

The corresponding forces and moments as a result of the induced oscillation are assumed harmonic in nature with the same frequency (Carlton 2018). The unsteady component of the hydrodynamic component is then written as:

$$q_H(t) = q_{H_x} sin(\omega \cdot t - \phi) \tag{5}$$

Where ϕ represents the phase difference between the motion and the propeller loading and q_{H_x} represents the resulting amplitude of unsteady torsional loading.

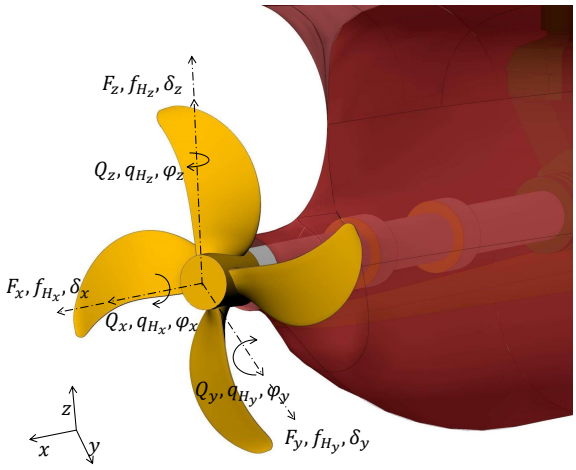

Figure 1: Vibration parameters for propulsion shafting

In the case of pure torsional vibration the axial motion x in Equation 3 is zero. Expanding this matrix equation with '$x = 0$' results in the following two equations:

$$m^*_{14}\ddot{\theta} + c^*_{14}\dot{\theta} = f_H sin(\omega t - \phi_1) \tag{6}$$

$$m^*_{44}\ddot{\theta} + c^*_{44}\dot{\theta} = q_H sin(\omega t - \phi_2) \tag{7}$$

The resulting added mass and damping coefficients are obtained as a result of algebraic and trigonometric manipulation. Moreover, the expressions for added mass and damping are non-dimensionalized in the following form:

$$m_{44} = \frac{m^*_{44}}{\rho D^5} \tag{8}$$

$$m_{14} = \frac{m^*_{14}}{\rho D^4} \tag{9}$$

$$c_{44} = \frac{c^*_{44}}{\rho n D^5} \tag{10}$$

$$c_{14} = \frac{c^*_{14}}{\rho n D^4} \tag{11}$$

2.2 Numerics

The propeller operation in a wakefield is simplified as a linear superposition of the propeller operating in a uniform flow and inducing a propeller vibration in a desired direction. The hydrodynamic forces and moments obtained as a result reflect the added mass and damping properties of the propeller.

The equations governing the physics of the OWT model include the Navier-Strokes equations and Continuity equation in 3D satisfying the conservation of momentum and mass respectively. These equations are first converted into Reynolds-averaged form and then solved using a finite volume-based method in ANSYS CFX. The Reynolds stresses as a result of averaging are modeled by using a two-equation eddy viscosity-based turbulence model, the k ω - SST turbulence model as provided by Menter (1993). To model the flow behavior near the wall/surface of the propeller, the built-in automatic wall functions in ANSYS CFX are utilized (CFX-Solver Theory guide 2011).

The Open Water Test (OWT) condition for the propeller contains an outer stationary domain and an inner rotating domain. Figure 2 shows the computational domain for the OWT case which is discretized using tetrahedral cells. In addition, inflation layers are added to the propeller to capture the near wall effects closer to the propeller surface. Figure 3 shows the mesh elements and Figure 4 represents the corresponding y^+ obtained for the OWT case.

The torsional motion is modeled by superimposing the harmonic velocity to the inner domain's rotation.

$$\dot{\theta}(t) = \dot{\theta}_0 sin(\omega \cdot t) + 2\pi n \tag{12}$$

Where $2\pi n$ represents the propeller rotation in rad/s. $\dot{\theta}_0 = \omega \cdot \theta_0$ represents the magnitude of the torsional vibration velocity and θ_0 is set to $\theta_0 = 5°$. Moreover, ω represents the excitation frequency and t is the time.

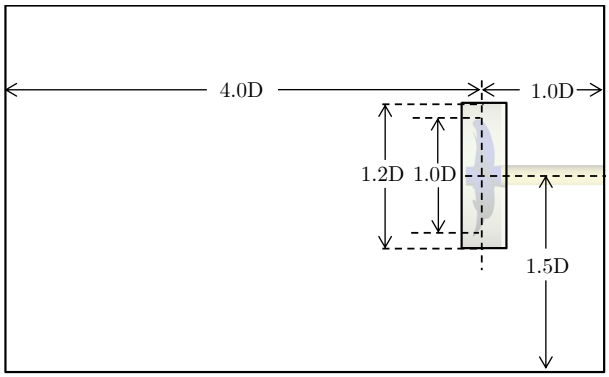

Figure 2: Domain dimensions in OWT condition

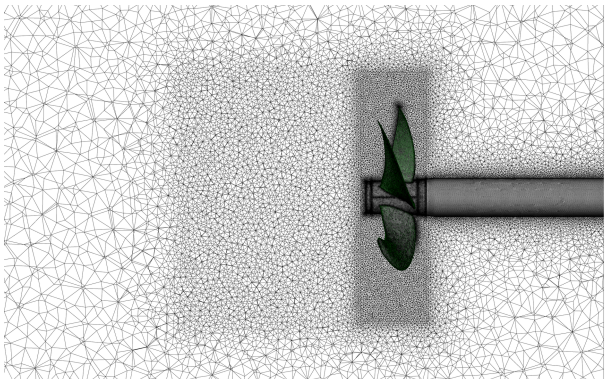

Figure 3: Side view of tetrahedral mesh elements

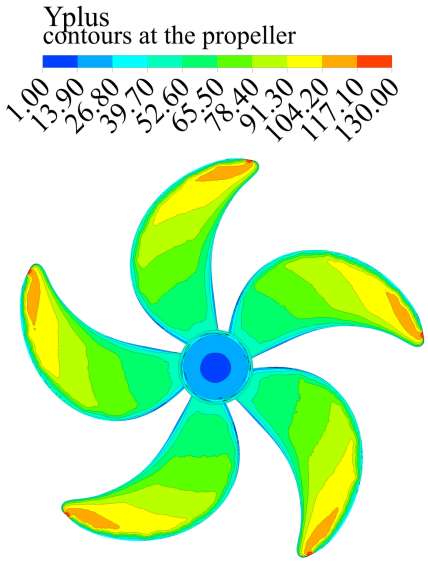

Figure 4: Dimensionless first cell height, y^+, contours for the propeller

The results are obtained in the form of propeller thrust and torque. These forces are transformed into non-dimensional entities:
$K_T = \frac{T}{\rho n^2 D^4}$, $K_Q = \frac{Q}{\rho n^2 D^5}$, $J = \frac{V_A}{nD}$, $ETA = \frac{K_T}{K_Q} \cdot \frac{J}{2\pi}$

2.3 Validation

An in-house propeller design is taken as a reference to validate and verify the CFD model for the OWT performance and to perform torsional vibration cases. The particulars of the propeller are shown in Table 1. Figure 5 shows the corresponding geometry.

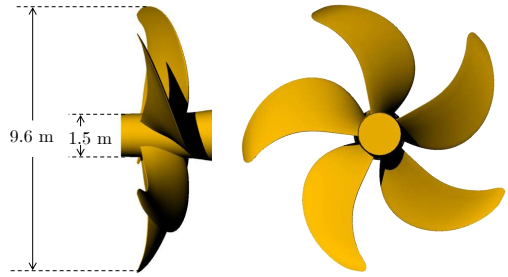

Figure 5: Full-scale propeller geometry

Table 1: Geometry parameters for the full scale marine propeller

Propeller Diameter	9.6	m
Hub diameter	1.5	m
P/D	1.083	[-]
EAR	0.584	[-]
Z	5	[-]

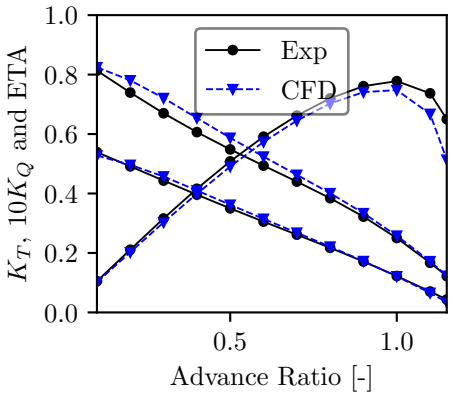

Figure 6: Propeller performance curve for full scale

The CFD results are compared with the available experimental data. Figure 6 shows the performance validation of the propeller. Good agreement is found between experimental and CFD results. Hence, the developed CFD model can predict propeller loading with good accuracy.

3 RESULTS AND DISCUSSION

3.1 Effect of vibration magnitude on propeller coefficients

In order to investigate the effect of torsional vibration magnitude on the added mass and damping coefficients, two torsional vibration cases are studied. Torsional vibration magnitudes of θ_0 = 1° and 5° are used with fe/BPF=1, $n = 1$ rps and J=0.9.

The propeller torque obtained due to the change in the vibration magnitude is shown in Figure 7. A difference in the magnitude is clearly visible. Similar behavior is observed with the thrust. The torque for $\theta_0 = 5°$ vibration magnitude is found to be higher in magnitude than for the $\theta_0 = 1°$ vibration magnitude case.

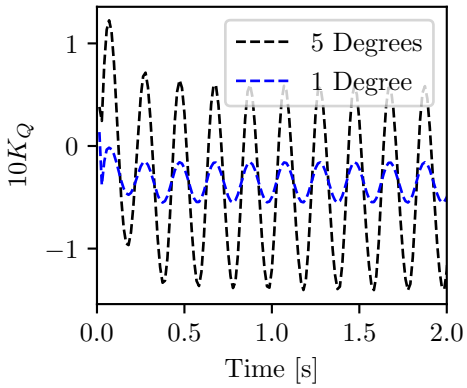

Figure 7: Propeller torque for two different vibration magnitudes

The magnitude of the non-dimensional torque amplitude for 5° is almost 5 times higher than 1° amplitude as can be observed in Table 2. The non-dimensional thrust amplitude depicts the same variation. Since the amplitude increases in an almost similar fashion as the magnitude of vibration, their ratio, and consequently the added mass and damping coefficients, remains the same for both cases as evident from Table 2.

Table 2: Propeller hydrodynamic forces and coefficients for different vibration magnitudes

Forces	$\theta_0 = 1°$	$\theta_0 = 5°$
K_T mean	0.133	0.159
$10K_Q$ mean	0.273	0.316
T (Non dimensional)	0.085	0.435
Q (Non dimensional)	0.151	0.767
Propeller Coefficients		
m_{44}	0.00080	0.00080
m_{14}	-0.00454	-0.00453
c_{44}	0.02636	0.02552
c_{14}	-0.16503	-0.15895

3.2 Excitation frequency

The effect of excitation frequency on the propeller loading parameters, torque and thrust, is analyzed in this section. The excitation frequency chosen for this study ranges from $fe/BPF = 0.2$ to $fe/BPF = 1.4$.

3.2.1 Propeller loading amplitudes

The propeller loading increased non-linearly when the excitation frequency increased. Figures 8 represents the torque and thrust amplitude variation with the excitation frequency respectively. Essentially, this loading is decomposed into added mass and damping forces according to Equation 2.

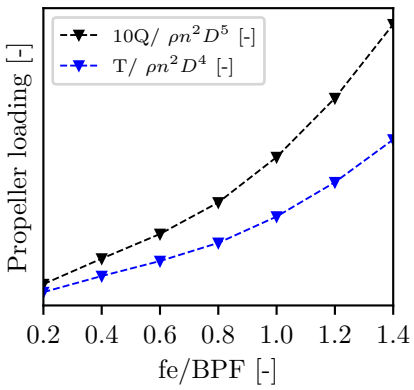

Figure 8: Effect of excitation frequency on the amplitude of torque and thrust loading

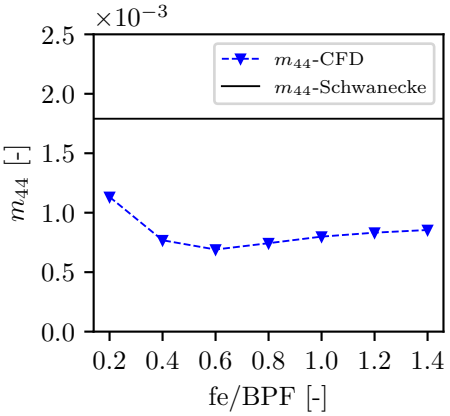

Figure 9: Effect of excitation frequency on m_{44}

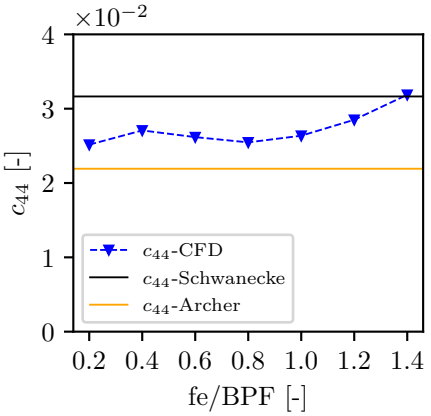

Figure 10: Effect of excitation frequency on c_{44}

3.2.2 Propeller added mass and damping coefficients

The contribution of the torque loading is decomposed into the diagonal added mass and damping coefficients. The resultant values are plotted in Figures 9 and 10 respectively.

The m_{44} value decreased exponentially at lower frequency ratios and approached a constant value when the frequency ratio was increased as shown in Figure 9. Closer and slightly higher to BPF, the variation of m_{44} is very minute.

When comparing with Schwanecke's semi-empirical formulations (Schwanecke 1963) in Figure 9, the results reveal that the CFD calculations produced smaller m_{44} values than Schwanecke. The difference of approximately 35% to 55% is observed for all ranges of excitation frequencies between Schwanecke's results and the current calculations which can significantly impact the accuracy of the computation of the natural frequency of the propulsion shafting system.

For the damping coefficient, c_{44}, the opposite trend is observed as compared to m_{44}, as seen in Figure 10. In general, it can be said that the coefficient remained almost constant at lower frequency ratios and increased exponentially at higher frequency ratios unlike m_{44}.

Moreover, the c_{44} values obtained from the current CFD calculations are lower than Schwanecke's value (1963), which is constant throughout the range of frequency ratios as it only depends on the propeller's geometrical parameters. However, at higher frequency ratios the values obtained by the CFD surpass Schwanecke's value for c_{44}. At the BPF, the difference between Schwanecke's results and the current CFD calculations for c_{44} is about 17%.

When comparing with Archer (1951), calculations showed that the damping values, c_{44}, are smaller for Archer than CFD. This suggests that the resulting torsional stresses will always be larger when using Archer's method which leads to an over-design of the shafting system. A relative difference of about 15% to 45% is observed between CFD and Archer values with about 20% difference observed at the BPF.

3.3 Advance ratio

The effect of advance ratios on the propeller's added mass and damping are investigated in this section. The advance ratio is varied between the values of 0.7 and 0.9 which represents the operational regime of the vessel.

Results reveal that no variation is observed for the propeller's added mass coefficient when the advance ratio is varied as shown in Table 3. This suggests that both m_{44} and m_{14} are independent of advance ratios in the given range. The same is the case with c_{44}. However, a small variation in c_{14} is observed with the advance ratio. Figures 11 and 12 provide a similar conclusion as the variation in the advance ratio, between the value of 0.7 and 0.9, results in no change in m_{44} and c_{44}.

Table 3: Effect of Advance Ratio on added mass and damping coefficients

	CFD			Schwanecke
	$J = 0.7$	$J = 0.8$	$J = 0.9$	
m_{44}	0.00081	0.00080	0.00080	0.0018
m_{14}	-0.00450	-0.00453	-0.00454	-0.0104
c_{44}	0.0266	0.0265	0.0264	0.0316
c_{14}	-0.176	-0.171	-0.165	-0.184

3.4 Pitch to diameter and expanded area ratio

The expanded area ratio (EAR) values used in this study

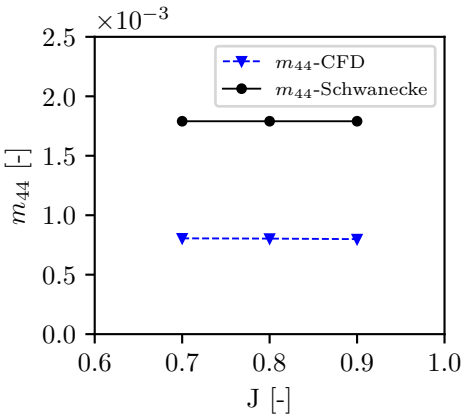

Figure 11: Effect of advance ratio on m_{44}

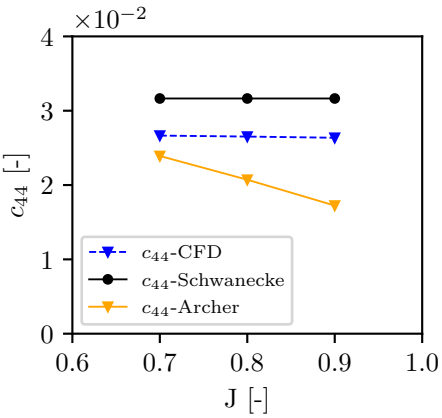

Figure 12: Effect of advance ratio on c_{44}

are EAR =0.5, 0.6, and 0.7, moreover, the pitch to diameter ratio (P/D) is varied between P/D =0.9, 1.0, and 1.1. The vibration magnitude is kept at $\theta = 5°$, and the excitation frequency as a ratio of BPF is kept at $fe/BPF = 1.0$ with the advance ratio of $J = 0.9$. Finally, the propeller rotation speed is kept unchanged at $n = 1$ rps.

Figure 13 shows the variation in the added mass m_{44} when P/D and EAR are varied. A nonlinear increment in m_{44} is evident from the figure when EAR is varied linearly for a given P/D. Moreover, Figure 14 shows the variation of c_{44} when P/D and EAR are varied. Contrary to m_{44}, the effect of EAR on c_{44} is almost linear. The added mass coefficient m_{44} for a given propeller EAR range is in between $m_{44} = 4.4 \cdot 10^{-4}$ for the lowest value of EAR and $m_{44} = 1.2 \cdot 10^{-3}$ for the highest value of EAR. Moreover, the change in m_{44} when EAR is varied is the same between any two P/D ratios. The damping coefficient, c_{44}, varies in between $c_{44} = 1.6 \cdot 10^{-2}$ and $c_{44} = 3.2 \cdot 10^{-2}$ for the available ranges of EAR as shown in Figure 14. Also, the variation of c_{44} remained almost the same for all values of P/D.

Comparing the variation of m_{44} for EAR and P/D, it is observed that EAR influences m_{44} more than P/D. The same cannot be said for c_{44}, where both EAR and P/D show the same proportion of increment when these variables are increased.

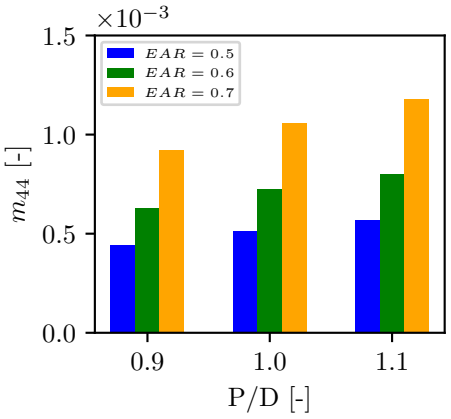

Figure 13: Effect of P/D and EAR on m_{44}

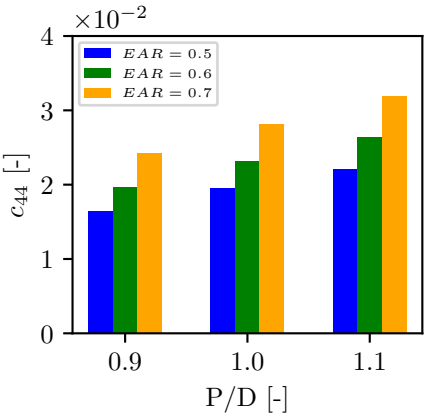

Figure 14: Effect of P/D and EAR on c_{44}

3.5 Propeller blade skew

For the added mass, a less skewed propeller increased the value of m_{44} as shown in Table 4. A relative difference of about 11% is observed between the high-skewed and low-skewed propellers. This effect of skew is not included in the semi-empirical formulation of Schwanecke (1963). The off-diagonal component of added mass decreased (increased in magnitude) when the skew was reduced. A difference of about 11%, similar to the difference in m_{44}, is observed for m_{14}.

Table 4: Summary of the effect of skew variation on added mass and damping coefficients

	$\theta_{Skew} = 20°$	$\theta_{Skew} = 36.4°$	≈Difference %
m_{44}	0.00089	0.00080	11.3
m_{14}	-0.00504	-0.00454	11.1
c_{44}	0.02738	0.02636	4.0
c_{14}	-0.17075	-0.16503	3.5

Similarly, the diagonal component of the damping matrix shows an increase when the skew is decreased from the

initial value of 36.4° to 20° as shown in Table 4. A relative difference of about 4% is observed for c_{44} between the two skewed propellers. Moreover, the off-diagonal damping term also decreases when the skew is reduced from the initial value as shown in Table 4. The value of c_{14} changed about 3.5% when the skew is reduced.

3.6 Four bladed propeller

Two propellers with different blade numbers are simulated for the added mass and damping coefficients. The vibration parameters are kept the same as before. The vessel speed for both cases is about $V_a = 19$ kn and the engine is rotating at about $n = 97$ rpm. Both propeller designs operate the ship at the same propulsion condition, so the propeller added mass and damping influence between both designs can be compared, and their influence on vibration can be concluded. The geometrical characteristics for both propellers are presented in Table 5.

The added mass and damping coefficient increased for the five-bladed propeller as compared to the four-bladed propeller. The major contribution of this variation is attributed mainly to the increase in EAR and P/D. As shown in Figure 13, increasing $EAR = 0.5$ to 0.6 increases m_{44} by about 38%. Assuming linear interpolation, an increase of $\Delta EAR = 0.06$ leads to about 23% increase in m_{44}. Similarly, an increase in $P/D = 0.89$ to 0.97 (with $EAR = 0.5$) leads to a 12% increase in m_{44}. Taking into account both parameters linearly, the total increment should be around 35%. However, the obtained increment (see Table 6) is about 13.4%. That depicts a 16% decrease in m_{44} that can be due to the effect of blade number. The behavior agrees with the available literature. For example, Schwanecke (1963) also proposed an inverse relation with the blade number for m_{44}.

Table 5: Propeller geometrical characteristics for four and five-bladed propellers

Parameters	Value	
	$Z = 4$	$Z = 5$
P/D	0.89	0.97
EAR	0.44	0.5
D $[m]$	7.3	7.0
Vessel Speed $[kn]$	18.29	18.71
rpm $[rps]$	1.61	1.61

Table 6: Comparison of the obtained propeller coefficient for four and five-bladed propellers

	$Z = 4$	$Z = 5$	$\approx$ Difference [%]
m_{44}	0.000499	0.000566	13.4
m_{14}	-0.00324	-0.00363	11.8
c_{44}	0.0160	0.0200	25.2
c_{14}	-0.114	-0.137	20.6

Similarly for c_{44}, an increase in EAR and P/D by 0.06 and 0.08 leads to a respective increase in c_{44} of about an 11% and 18%, as shown in Figure 14. Taking account of both would lead to an overall 29% increase in c_{44}. However, the obtained difference is about 25% leading to a variation of about 3% that can be due to the effect of the blade number. Moreover, Schwanecke's (1963) formulation for c_{44} is independent of the blade number.

4 CONCLUSION

A RANS CFD framework is developed to obtain the added mass and damping coefficients for torsional vibration. The effect of the non-uniform wake field on the propeller due to the ship hull was modeled by superimposing a harmonic oscillation of the propeller with a uniform flow.

Results showed that the added mass and damping coefficients for torsional vibration remained the same when the magnitude of oscillation and advance ratio were varied. Excitation frequency varied the hydrodynamic thrust and torque in a nonlinear way.

Moreover, the added mass and damping coefficients show a non-linear behavior when the excitation frequency is varied. The result demonstrated a strong effect of the propeller EAR on m_{44} as compared to P/D. The damping coefficients, c_{44}, varied linearly with the propeller EAR and P/D.

Results show that the skew has an inverse effect on the added mass and damping coefficients for torsional vibration. An increase in blade number for a given ship with a similar engine and ship speed leads to a decrease in both added mass and damping coefficients.

Finally, the developed CFD framework can be utilized in torsional vibration calculations (TVC) where the obtained added mass and damping coefficients are used to accurately calculate the frequency and torsional stress response of the propulsion shafting system respectively.

ACKNOWLEDGMENTS

This paper is derived from the master thesis within the framework of the Erasmus Mundus master's program 'European Master's Course in Advanced Design of Ships and Offshore Structures (EMShip+)'.

REFERENCES

Archer, S. (1951). 'Contribution to improved accuracy in the calculation and measurement of torsional vibration stresses in marine propeller shafting'. Proceedings of the Institution of Mechanical Engineers. 164(1), 351-366.

Burrill, L. C., & Robson, W. (1962). 'Virtual mass and moment of inertia of propellers'. The North East Coast Institution of Engineers and Shipbuilders, Bolbec Hall, Newcastle upon Tyne, UK, Institution Transactions.

Carlton, J (2018) Marine propellers and propulsion. 4th ed. Butterworth-Heinemann Book Company

CFX-Solver, ANSYS Theory guide, Release l4, 2011

Gaschler, M., & Abdel-Maksoud, M. (2014). 'Computation of hydrodynamic mass and damping coefficients for a cavitating marine propeller flow using a panel method'. Journal of Fluids and Structures, 49, 574-593.

Hyloarides, S., & Van Gent, W. (1979). 'Hydrodynamic reactions to propeller vibrations'. Schip en Werf, 46.

Lewis, F. M., & Auslaender, J. M. (1960). 'Virtual inertia of propellers'. Journal of Ship Research, 3(4), 37-46.

Li, J., Qu, Y., Chen, Y., & Hua, H. (2018). 'Investigation of added mass and damping coefficients of underwater rotating propeller using a frequency-domain panel method'. Journal of Sound and Vibration, 432, 602-620.

Mao, Y., & Young, Y. L. (2016). 'Influence of skew on the added mass and damping characteristics of marine propellers'. Ocean Engineering, 121, 437-452.

Martio, J., Sánchez-Caja, A., & Siikonen, T. (2015, June). 'Evaluation of propeller virtual mass and damping coefficients by URANS-method'. In Fourth International Symposium on Marine Propulsors smp'15.

Martio, J., Sánchez-Caja, A., & Siikonen, T. (2017). 'Open and ducted propeller virtual mass and damping coefficients by URANS-method in straight and oblique flow'. Ocean Engineering, 130, 92-102.

Menter, F. (1993, July). 'Zonal two equation kw turbulence models for aerodynamic flows'. In 23rd fluid dynamics, plasmadynamics, and lasers conference, (p. 2906).

Parsons, M. G., Vorus, W. S., & Richard, E. M. (1980). 'Added mass and damping of vibrating propellers'. University of Michigan.

Schwanecke, H. (1963). 'Gedanken zur Frage der Hydrodynamisch erregten Schwingungen des Propellers und der Wellenleitung'. Versuchsanstalt für Wasserbau und Schiffbau,Berlin Berlin, Sonderdruck aus Jahrbuch der Schiffbautechnischen Gesellschaft, Band 57, 1963.

Van Esch, B. P. M., Van Hooijdonk, J. J. A., & Bulten, N. W. H. (2013, July). 'Quantification of hydrodynamic forces due to torsional and axial vibrations in ship propellers'. In Fluids Engineering Division Summer Meeting. American Society of Mechanical Engineers, Vol. 55553, pp. V01BT10A025.